Solar Energy Materials and Solar Cells 178 (2018) 179–185

Contents lists available at ScienceDirect

Solar Energy Materials and Solar Cells

journal homepage: www.elsevier.com/locate/solmat

Electrical and optical degradation study of methylammonium-based perovskite materials under ambient conditions

Arthur Marronnier[a,*], Heeryung Lee[a], Heejae Lee[a], Minjin Kim[a], Céline Eypert[b], Jean-Paul Gaston[b], Guido Roma[c], Denis Tondelier[a], Bernard Geffroy[a,d], Yvan Bonnassieux[a]

[a] LPICM, CNRS, Ecole Polytechnique, Université Paris-Saclay, 91128 Palaiseau, France
[b] Horiba Jobin Yvon S.A.S., 91120 Palaiseau, France
[c] DEN - Service de Recherches de Métallurgie Physique, CEA, Université Paris-Saclay, 91191 Gif sur Yvette, France
[d] LICSEN, NIMBE, CEA, CNRS, Université Paris-Saclay, 91191 Gif sur Yvette, France

ARTICLE INFO

Keywords:
Perovskite solar cells
Degradation
Aging
Ellipsometry
Dielectric constant
DFT

ABSTRACT

Hybrid perovskites have emerged over the past five years as absorber layers for novel high-efficiency low-cost solar cells which combine the advantages of organic and inorganic semiconductors. One of the main obstacles to their commercialization is their poor stability under light, humidity, oxygen, and high temperatures. In this work, we compare the optical and the electrical light-induced degradation of $CH_3NH_3PbI_3$ ("MAPI")-based solar cells using real-time ellipsometry measurements, electrical measurements and X-Ray Diffraction (XRD) techniques. We evidence that while the electrical degradation takes place on a short time scale (2–3 days of exposure to ambient light conditions in a nitrogen atmosphere), no optical degradation is observed before 10 days when the dissociation reaction of methylammonium lead iodide starts acting. We find a very good agreement between XRD and ellipsometry measurements; both show the appearance of PbI_2 after 1 week of exposure. We also confirm that the main mechanism at play is a light-induced degradation affecting the edges of the stack and the interfaces between the perovskite and the neighbouring layers. Last, a very good match is obtained on the optical constants of MAPI between our ellipsometry measurements and density functional theory calculations we performed, and we confirm the behavior of MAPI as an inorganic semiconductor.

1. Introduction

Even though the efficiency of hybrid perovskite solar cells (PSCs) has jumped from 4% in 2009 to certified efficiencies over 20% [1] in 2015 and a record efficiency of 22.7% [2] in 2017, the mechanisms behind their fast degradation have yet to be fully understood. Long-term stability, in particular in terms of efficiency, is a crucial point for any photovoltaics technology to reach the market.

Niu et al. [3] gave a first general understanding of the possible pathways of the chemical decomposition of the perovskite layer in 2015. This fast degradation has been attributed to different factors, among them: humidity, temperature, oxygen, and light [4]. While many studies focused on the role played by H_20 molecules in air [5], the mechanism behind ambient light-induced degradation remains unclear. Ito and co-workers [6] used UV–Vis absorption and X-Ray Diffraction (XRD) to show that after 12 h of light exposure, $CH_3NH_3PbI_3$ ("MAPI" or $MAPbI_3$) transformed into PbI_2, evidenced by the decreased UV–Vis absorption and XRD patterns. A possible mechanism to explain this degradation process is [6]:

$$2I^- = I_2 + 2e^- \quad (1a)$$

$$3CH_3NH_3^+ = 3CH_3NH_2 \uparrow + 3\,H^+ \quad (1b)$$

$$I^- + I_2 + 3\,H^+ + 2e^- = 3HI\uparrow \quad (1c)$$

The evolution of the optical properties of hybrid perovskite thin films with time can be followed using real-time spectroscopic ellipsometry techniques [7]. Shirayama et al. [8] used this method, together with Density Functional Theory (DFT) calculations, to investigate the degradation of $CH_3NH_3PbI_3$ upon exposure to humid air.

In this paper, we compare the optical and the electrical light-induced degradation of $CH_3NH_3PbI_3$-based solar cells using real-time ellipsometry measurements, electrical measurements and X-Ray Diffraction (XRD) techniques. Electrical characterization is performed on devices with a full solar cell structure using PEDOT-PSS as a hole transporting layer, and PCBM (Phenyl-C61-Butyric acid Methyl ester) as an electron transporting layer (see Section 2.1 for details). Ellipsometry

* Corresponding author.
E-mail address: arthur.marronnier@polytechnique.edu (A. Marronnier).

https://doi.org/10.1016/j.solmat.2018.01.020
Received 19 November 2017; Received in revised form 5 January 2018; Accepted 14 January 2018

and XRD are performed on a stack consisting of all the layers up to the perovskite layer. We followed the degradation with ellipsometry for 17 days and 2–3 measurements per day.

In order to focus on light-induced degradation, the first measurements were made while keeping the cells in a nitrogen atmosphere, even during the ellipsometry characterization (see Section 2.1). We also performed complementary ellipsometry measurements both in the dark and in air, to check if the degradation measured here could result from other factors than ambient light. We found out that keeping the cell in a nitrogen atmosphere does not seem necessary in order to study the light-induced degradation. Unless otherwise specified, the degradation studies reported here are made on layers prepared by evaporation. Additional studies on solution-processed samples are shown for comparison.

We also perform Density Functional Theory (DFT) calculations to get ab-initio values for the optical constants of MAPI. In particular, we study in detail in Section 3.3 its dielectric properties. The dielectric constant in the high-frequency regime (taking into account only electronic contribution) is obtained as a second derivative of energy with respect to electric fields. The dielectric function in the visible range is computed in the Random Phase Approximation (RPA) from KS eigenvalues and eigenvectors and compared to ellipsometry measurements we performed under a nitrogen atmosphere (see Section 2.2 for computational details).

As for the static dielectric constant (low frequency regime), ionic contributions are taken into account through the coupling of phonons with the electric field. The phonons are obtained by using the linear response approach of DFT, as known as DFPT (Density-Functional Perturbation Theory), see Section 2.2. Given the structural instability and the anharmonicity behavior previously reported for halide perovskites [9–12], we made sure to properly relax the structure to avoid soft phonon modes.

The PSC community has for some time had trouble agreeing on MAPI's exciton binding energy, and on whether it behaves more like organic compounds (high exciton binding energy, low dielectric constant) or vice-versa like inorganic compounds. We use here the phonon spectrum obtained for the pseudocubic phase of $MAPbI_3$ to confirm that it behaves as an inorganic semiconductor.

2. Experimental and computational methods

2.1. Experimental

For solution process, the analyzed samples consist of layers of (from bottom to top) glass, ITO, PEDOT: PSS and $MAPbI_xCl_{1-x}$, the latter two made under a nitrogen atmosphere. The ITO coated glass is patterned using a wet etching process with zinc powder and HCl, cleaned with deionized H_2O (DI water), acetone and isopropanol. A PEDOT: PSS (40 nm thick) hole transport layer is deposited on the ITO substrate using a spin-coating process and heated at 120 °C for 20 min in N_2 conditions. A perovskite solution (in DMF) composed of PbI_2, $PbCl_2$ and MAI with a 1:1:4 molar ratio is spun at 6000 r.p.m onto the PEDOT: PSS layer and heated at 80 °C for 2 h in N_2 conditions. The thickness of the obtained perovskite film is estimated to be 350–400 nm. We then deposited a filtered PCBM solution by spin coating (1-step process: 3000 rpm for 35 s) in the glove box (N_2 condition), and, without annealing, we deposited the Ag cathode using thermal evaporation.

For evaporation process, the analyzed samples also consist of layers of (from bottom to top) glass, ITO, PEDOT: PSS and $MAPbI_3$, the latter two made under a nitrogen atmosphere. ITO and PEDOT: PSS are prepared in the same way as for solution-processed cells. Then, the perovskite layer (around 250 nm) is deposited by thermal co-evaporation of MAI and PbI_2 with a 3:1 ratio on the PEDOT: PSS films. The evaporation rate is controlled by temperature through different parameters (current, voltage). In order to avoid a penetration of MAI inside the PEDOT: PSS layer, a thin layer (around 10–30 nm) of pure PbI_2 is deposited prior to co-evaporation. After breaking the vacuum and cooling, we annealed the perovskite thin films at 80 °C for 1 h under a nitrogen atmosphere. PCBM and Ag were deposited the same way as in the solution process.

The samples are scanned by a UVISEL, a phase-modulated spectroscopic ellipsometer (HORIBA) with an incidence angle of 60 °C and a wavelength range of 0.6–4.6 eV (270–2100 nm). As MAPI is a direct transition semiconductor (in the first order approximation), the Tauc-Lorentz [13] formula is used to extract the optical constants of the perovskite layer, after having extracted PEDOT: PSS and ITO optical constants with Glass/ITO/PEDOT: PSS samples beforehand. The ellipsometry fitting parameter χ^2 is kept under 15, as it is usually the case in order to have a good match between our model and the actual optical parameters [13]. The study of the bottom layers allows to concentrate our efforts only on the perovskite. Thanks to a sealed box, the samples are kept in a N_2 atmosphere during the first ellipsometry measurements, but this seemed to be unnecessary as it did not influence the optical light-induced degradation.

For t < 6 days, the perovskite film is modeled using three layers to take into account the variation of index in the depth and a surface roughness layer (see Fig. 1). These 3 layers are described using the Bruggeman Effective Medium Approximation, which consists of a mix of $MAPbI_3$ and void, whose volume fraction varies for the bulk perovskite and the bottom layer. The surface roughness is described with 50% of $MAPbI_3$ and 50% of void as introduced by Aspnes et al. [14]. The volume fraction of $MAPbI_3$ decreases day by day for both layers and more importantly for the bottom layer.

For t > 6 days, the perovskite film is still modeled using 3 layers with variation of the different volume fractions for each layer from the bottom to the top. In addition, we included a fraction of PbI_2 in these layers (see Fig. 2).

The optical transitions of the perovskite thin film are reported in the Supporting Information file and are coherent with the literature [7].

The absorbance is measured using a UV–Vis spectrophotometer. Given the wavelength range where the signal is not saturated (500–800 nm), the only optical transition which can be followed day after day is the band gap one around 1.57 eV.

The XRD measurements were carried out on samples exposed to ambient light and done at regular times from right after fabrication to after 6 weeks of exposure. The incident angle was increased from 5° to 75° by steps of 0.03°.

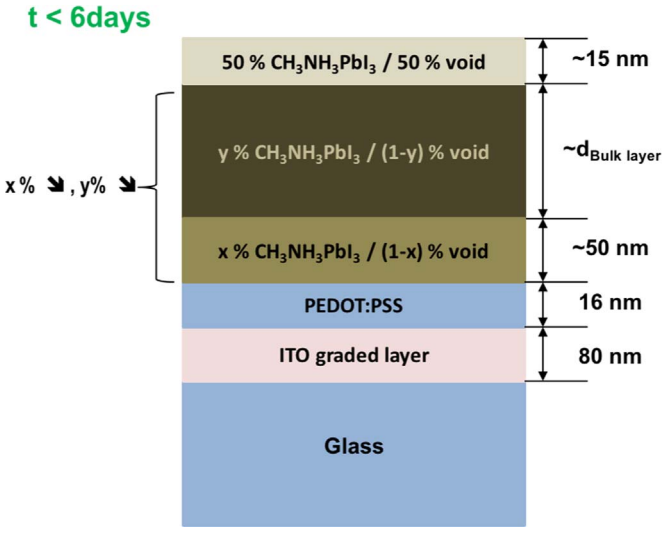

Fig. 1. Model used to fit the optical constants during the first 6 days of ageing. Layers are numbered starting from glass (L1) to the top (L6).

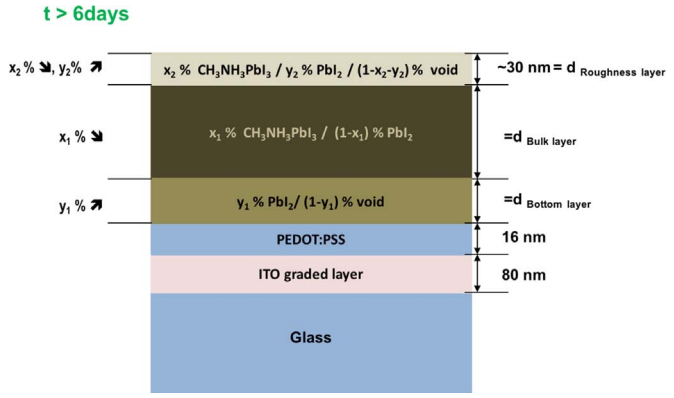

Fig. 2. Model used to fit the optical constants after the first 6 days of ageing. Layers are numbered starting from glass (L1) to the top (L6).

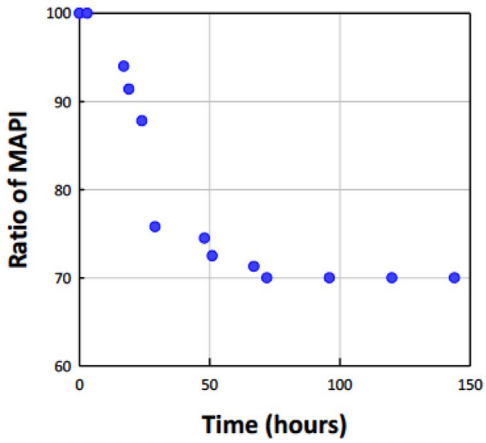

Fig. 3. Study over time of the ratio of MAPI (in %) under ambient light and nitrogen atmosphere conditions, after introducing a MAPI/void mixed layer in the ellipsometry model.

2.2. Computational methods

Electronic-structure calculations were performed within the Density-Functional Theory (DFT) [15,16] framework, as implemented in the Quantum Espresso (QE) code [17].

All total energy and force calculations in this work were performed with the Local Density Approximation (LDA), expanding the wave functions in a plane-wave basis set. Unless specified differently, non-relativistic (scalar-relativistic for Pb) and norm-conserving pseudopotentials were used, with the Cs $[5\,s^2 5p^6 6\,s^1]$, I $[5\,s^2 5p^5]$ and Pb $[5d^{10} 6\,s^2 6p^2]$ electrons treated as valence states.

Plane-wave cutoffs of 80 Ry were used. The Brillouin zone (BZ) was sampled with Γ-centered Monkhorst-Pack meshes [18] with a subdivision of 8 × 8 × 8. Dielectric functions were calculated with the epsilon.x tool of the post-processing suite of QE, in the framework of the RPA, neglecting local field effects.

Phonon calculations were performed using the linear response approach of DFT, as known as DFPT (Density-Functional Perturbation Theory) [19], as implemented in the Quantum Espresso code [17]. High-frequency dielectric tensors and Born effective charges were calculated with linear response and used to calculate long range contributions to the dynamical matrices at Γ.

In order to eliminate some of the soft phonon modes, very tight convergence thresholds of $10^{-4} Ry/bohr$ for the force calculations and 10^{-14} for the phonon self-consistent algorithm were used, similar to our previous work [9].

3. Results and discussion

3.1. The first 6 days: Electrical degradation

In order to optimize the optical parameters obtained by ellipsometry during the first 6 days, we propose a model where we increase the void ratio in the MAPI layer so that the fitting parameter χ^2 is kept under 15 (see Section 2.1 for details). The results (Fig. 3) show that light-induced degradation manifests through a void ratio increasing from 0% to 30% within 3 days in the MAPI layer. The fact that such a model with only void taken into account fits the experimental optical constants means that no PbI_2 is expected to be formed during the first 6 days of exposure to light.

In parallel, we studied the electrical degradation of complete solar cells by measuring their IV characteristics over time when exposed to ambient light and nitrogen atmosphere (see Figs. 4 and 5). The electrical degradation acts very fast since the Power Conversion Efficiency (PCE) drops from 7.4% to around 4% after only 2 days for the cells made by co-evaporation. The major degradation occurs for the short circuit current (J_{SC}) and the series resistance (R_{series}). We think that the abrupt drop of series resistance (see detailed data in the Supporting Information file) could be the sign of a degradation occurring mostly at the interfaces with other layers, as opposed to modifications in the bulk of the perovskite layer. We show in Fig. 4 (b), for comparison, the electrical degradation which occurs when the samples are exposed to both ambient light and air. The degradation in air occurs at an even higher rate than in nitrogen.

In contrast, Fig. 5 shows the electrical degradation of cells prepared using solution process instead. For such cells, the initial substantial drop in performance occurs after only 2 days, but they show better stability as J_{SC} only slightly decreases during the following 10 days.

In order to confirm the ellipsometry results showing no appearance of PbI_2 during the first 6 days of exposure, we also performed UV–Vis spectroscopy measurements. No change was observed in the optical absorption transitions. Moreover, the color of the samples did not turn to yellow, but rather remain dark brown during the first 6 days of degradation (see Fig. 6).

All these results show that whereas no optical degradation is observed for 6 days, the electrical degradation due to ambient light is very fast and the cells lose their electrical properties after only 2 days.

3.2. From day 6 to day 12: Lead iodide formation

Starting from day 6, we had to use a different ellipsometry model and include a fraction of PbI_2 in the MAPI layer in order to maintain a faithful model of the optical parameters (see Section 2.1). The results (Fig. 7 for t > 120 h) show that this fraction increases rapidly to more than 80% after 9–10 days. This results from the dissociation reaction of MAPI into its precursor elements lead iodide and methylammonium, as previously reported [6]. The ratio of PbI_2 reaches a limit value of approximately 88% and does not increase anymore from day 10 to day 17.

This is further confirmed by XRD measurements we performed (see Fig. 8), clearly showing the appearance of a PbI_2 peak after 1 week of exposure.

Last, the real part of the dielectric constant ϵ of the MAPI layer extracted from ellipsometry is shown in Fig. 9. Noteworthy, this data reveals that the degradation mechanism which is at play here is much faster during the day (ambient light) than during the night. This can be seen as the major changes for ϵ are observed for measurement points close to each other, which correspond to daylight conditions (see Section 2.1). This further strengthens our study and validate our approach of studying the degradation of perovskite stacks caused by ambient light. Similarly, no degradation was observed after keeping one of the samples wrapped in aluminum foil for 15 days.

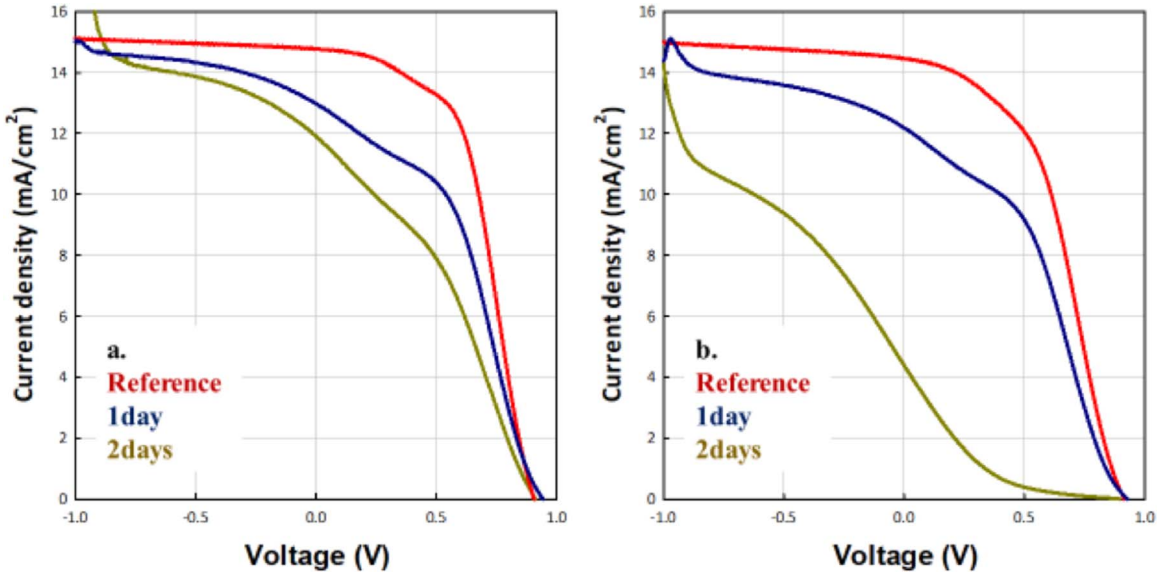

Fig. 4. Study over time of the electric properties of MAPI-based perovskite solar cells prepared by evaporation, under ambient light and nitrogen atmosphere conditions for (a) and exposed to air for (b).

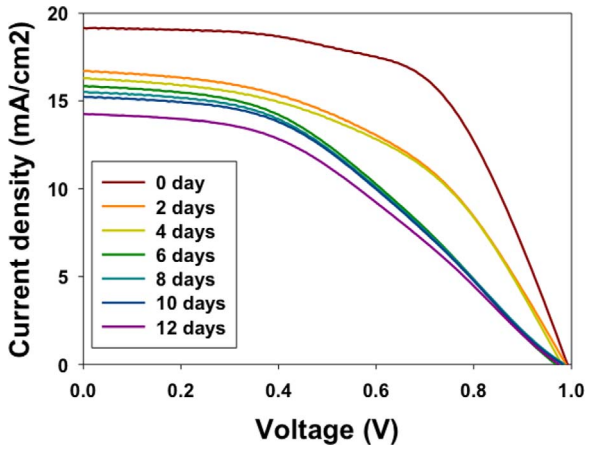

Fig. 5. Study over time of the electric properties of MAPI-based perovskite solar cells, prepared by solution process, under ambient light and nitrogen atmosphere conditions.

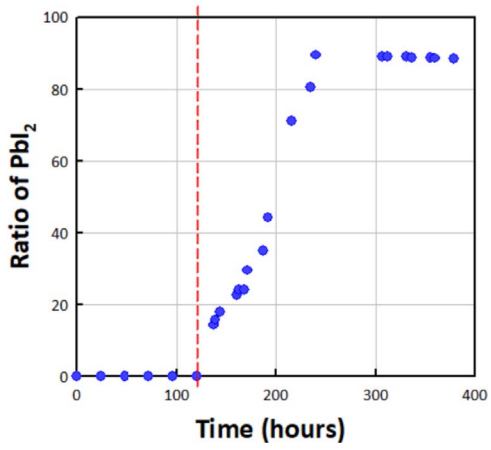

Fig. 7. Study over time of the ratio of PbI_2 (in %) in the MAPI layer under ambient light and nitrogen atmosphere conditions. The different model used for t < 120 hours sets x = 0 by definition (see Section 2.1) and is shown here for comparison.

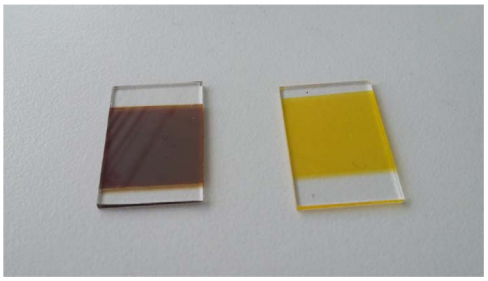

Fig. 6. MAPI-based perovskite solar cells (without the top electrodes), exposed to ambient light and kept in a nitrogen atmosphere, after 6 days (left) and 8 days (right) of degradation.

3.3. DFT analysis

The aim of our DFT analysis was to obtain the dielectric properties of $MAPbI_3$ (using its phonon spetra) and compare them to the dielectric function measured by ellipsometry.

As we previously reported [9], contrary to $CsPbI_3$, the phonon spectrum of the pseudocubic phase of the hybrid perovskite $MAPbI_3$, obtained using DFPT calculations, does not have any soft modes at the Γ point of the Brillouin zone. This means that, provided that we use a very tight convergence threshold for the DFT relaxation, we can reach the proper equilibrium structure without the use of frozen phonon calculations.

From this phonon spectrum free of soft modes, we could derive the static dielectric constant ϵ_0. The frequency dependent dielectric function is obtained within the RPA by calculating the proper coefficients of each allowed transition between states v in the valence band and states c in the conduction band [20]:

$$\epsilon_1(\omega) = 1 + \sum_{c,v} f_{c,v} \frac{\omega_p^2}{\omega_{c,v}^2 - \omega^2} \tag{2a}$$

$$\epsilon_2(\omega) = \frac{\pi}{2} \sum_{c,v} f_{c,v} \frac{\omega_p^2}{\omega} \delta(\omega - \omega_{c,v}) \tag{2b}$$

$\omega_{c,v}$ being the transition's oscillator frequency, and ω_p the plasma frequency of the solid.

The static and high frequency dielectric constants of pseudocubic $MAPbI_3$ obtained with DFPT are:

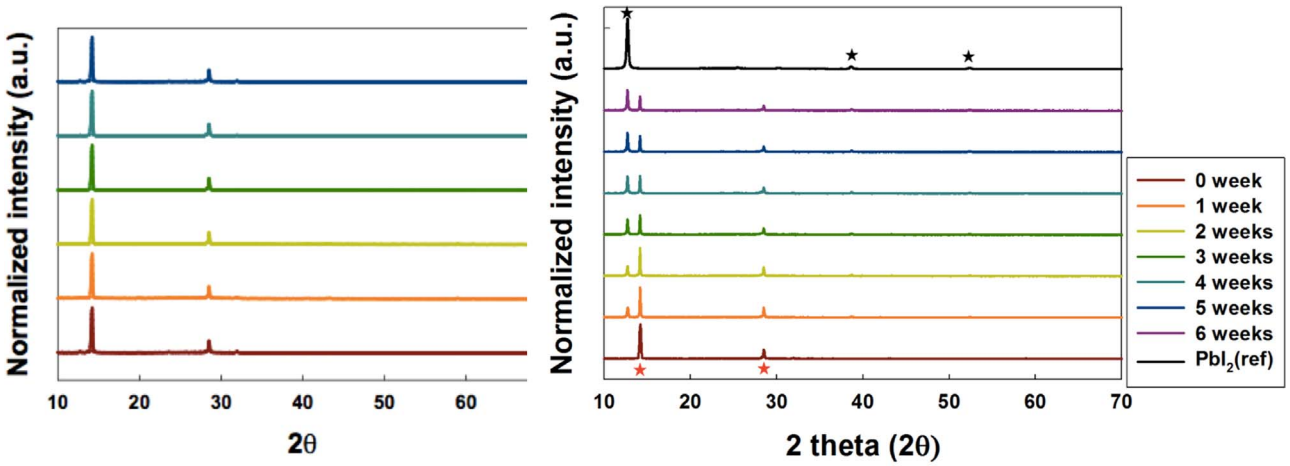

(a) First 5 days of ageing.

(b) 6 weeks of ageing. Red and black stars represent respectively the peaks attributed to the MAPI and PbI_2 crystals.

Fig. 8. X-ray diffraction spectrum of MAPI stacks kept under a nitrogen atmosphere in ambient light.

$$\epsilon_0 = \begin{bmatrix} 14.49 & 0.06 & -0.59 \\ -0.06 & 17.64 & 0.04 \\ -0.59 & 0.04 & 18.70 \end{bmatrix} \epsilon_\infty = \begin{bmatrix} 6.19 & 0.00 & -0.22 \\ 0.00 & 6.30 & 0.00 \\ -0.22 & 0.00 & 6.44 \end{bmatrix} \quad (3)$$

The results obtained (static ϵ around 18) are coherent with low exciton binding energies, but go against the possibility of a giant dielectric constant for these hybrid perovskites, which had been reported at very low frequencies (<1 Hz) (ϵ ≈ 1000 in the dark [21]). They are also reasonably close to the previously reported experimental value of 30.5 [22].

The dielectric function (ϵ versus energy, Fig. 10a), calculated in the visible range, shows good concordance with the ellipsometry measurements (Fig. 10b). The real part of the dielectric function measured by ellipsometry has the same order of magnitude before the transition (5–6) as the calculated values shown in Eq. (3). The calculated imaginary part, representing the absorption of the perovskite layer, is slightly shifted to lower energies compared to ellipsometry measurements, showing an optical band gap of around 1.2 eV compared to 1.56 eV for ellipsometry. This is actually highly dependent on the smearing value chosen to calculate the different f_{cv} oscillation strength factors (see Eqs. (2a) and (2b)).

In the Supporting Information file we show that one can play with this smearing value: the lower the smearing, the closer the band gap is to the experimental value, but also the more noise there is in the dielectric function. Check-up ab initio calculations were performed (see Supporting Information) to make sure our relaxed structure has the expected band gap, and we found a value 1.57 eV with ultrasoft pseudopotentials, this value being close to experimental values only because of a now well-known for these perovskites [23] error cancellation between the underestimation of DFT and the effect of spin orbit coupling which we do not take into account here.

In general, we think that the differences observed between Fig. 10a and 10b can be explained by several reasons. One of them is the roughness of the perovskite layer. Shirayama et al. [7] showed that ultrasmooth perovskite layers (prepared using a laser evaporation technique) can produce artifact-free measurements of $MAPbI_3$ optical constants, with an almost perfect agreement with DFT. Another reason can be the fact that our calculations are performed on the pseudocubic phase, of $MAPbI_3$ whereas the stable phase at room temperature is the tetragonal phase.

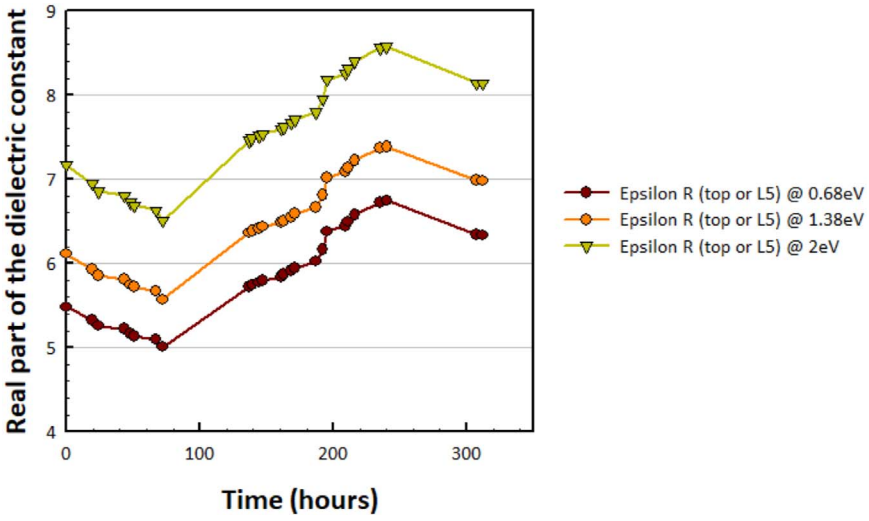

Fig. 9. Study over time of real part of the dielectric constant of the MAPI layer, as modeled from ellipsometry measurements. Close points corresponds to measures during the day, while distant points are separated by at least one night of exposure. See Section 2.1 for a detailed explanation about the layers labelling (L1 to L6).

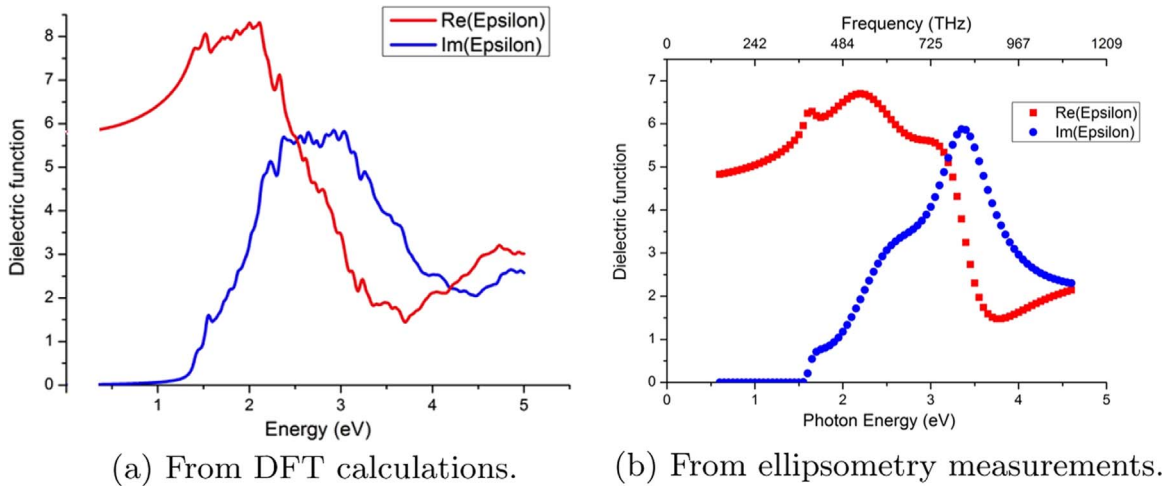

Fig. 10. Dielectric function of $MAPbI_3$.

4. Concluding remarks

To summarize, we can draw two main conclusions from our degradation study under nitrogen and ambient light conditions.

First, the electrical degradation occurs on a very fast time scale: after only 2 or 3 days, the perovskite cells are almost not generating power anymore, whereas their optical absorption properties are stable at this time scale (both the optical transitions measured by UV–Vis spectroscopy and the optical constants n and ϵ obtained by ellipsometry).

Second, the dissociation reaction leading to the formation of lead iodide can be probed by fitting the optical constants obtained by ellipsometry with models including a growing ratio of PbI_2 in the MAPI layer. This model shows that the formation of lead iodide does not start before day 6, which is coherent with the stack turning yellow only after the first 6 days of exposure to light, and that the fraction of lead iodide in the MAPI layer increases until reaching a saturation value of around 90% after 9–10 days.

Using additional DFT calculations on the dielectric constants, which are in good agreement with the optical constants measured by ellipsometry, we are able to confirm the behavior of MAPI as an inorganic semiconductor with a high static dielectric constant and thus low values for the exciton binding energies.

These findings highlight the crucial importance of inhibiting the mechanisms responsible for light degradation, in addition to protecting them from oxygen, humidity and temperature, since even under a nitrogen atmosphere, the light-induced degradation is crippling for the solar cell's performance.

Further work is needed to investigate in detail the dynamics of such degradation, and especially the different mechanisms at play for the very fast electrical degradation on one hand and the slower optical degradation on the other hand.

5. Author information

5.1. Notes

The authors declare no competing financial interest.

Acknowledgements

Arthur Marronnier's PhD project is funded by the French Department of Energy (MTES) and by the Graduate School of École des Ponts ParisTech.

This work was granted access to the HPC resources of TGCC and CINES under allocation 2016090642 made by GENCI.

The authors would also like to thank A. Garcia Barker for her editing and proofreading contributions.

Appendix A. Supporting information

SI.pdf: this supporting information file is devoted to presenting some checks we made in order to show that the main differences between the DFT calculated dielectric function of MAPI and the one measured by ellipsometry measurements (see Figs. 10a and 10b) are linked to numerical artifacts and do not affect the conclusions of the paper.

We also provide detailed data about the electrical degradation and show a comparison between the dielectric properties of solution-processed and co-evaporated perovskite thin films.

Appendix B. Supplementary data

Supplementary data associated with this article can be found in the online version at http://dx.doi.org/10.1016/j.solmat.2018.01.020.

References

[1] W.S. Yang, J.H. Noh, N.J. Jeon, Y.C. Kim, S. Ryu, J. Seo, S.I. Seok, High-performance photovoltaic perovskite layers fabricated through intramolecular exchange, Science (2015) 0036–8075.

[2] Best Research-cell Efficiencies, 2017. (Accessed 17 October 2017)〈https://www.nrel.gov/pv/assets/images/efficiency-chart.png〉.

[3] G. Niu, X. Guo, L. Wang, Review of recent progress in chemical stability of perovskite solar cells, J. Mater. Chem. A 3 (2015) 8970–8980.

[4] D. Wang, M. Wright, N.K. Elumalai, A. Uddin, Stability of perovskite solar cells, Sol. Energy Mater. Sol. Cells 147 (2016) 255–275.

[5] J.H. Noh, S.H. Im, J.H. Heo, T.N. Mandal, S.I. Seok, Chemical management for colorful, efficient, and stable inorganic-organic hybrid nanostructured solar cells, Nano Lett. 13 (2013) 1764–1769.

[6] S. Ito, S. Tanaka, K. Manabe, H. Nishino, Effects of surface blocking layer of sb_2s_3 on nanocrystalline tio_2 for $ch_3nh_3pbi_3$ perovskite solar cells, J. Phys. Chem. C 118 (2014) 16995–17000.

[7] M. Shirayama, H. Kadowaki, T. Miyadera, T. Sugita, M. Tamakoshi, M. Kato, T. Fujiseki, D. Murata, S. Hara, T.N. Murakami, S. Fujimoto, M. Chikamatsu, H. Fujiwara, Optical transitions in hybrid perovskite solar cells: ellipsometry, density functional theory, and quantum efficiency analyses for $ch_3nh_3pbi_3$, Phys. Rev. Appl. 5 (2016) 014012.

[8] M. Shirayama, M. Kato, T. Miyadera, T. Sugita, T. Fujiseki, S. Hara, H. Kadowaki, D. Murata, M. Chikamatsu, H. Fujiwara, Degradation mechanism of $ch_3nh_3pbi_3$ perovskite materials upon exposure to humid air, J. Appl. Phys. 119 (2016) 115501.

[9] A. Marronnier, H. Lee, B. Geffroy, J. Even, Y. Bonnassieux, G. Roma, Structural instabilities related to highly anharmonic phonons in halide perovskites, J. Phys. Chem. Lett. 8 (2017) 2659–2665.

[10] L.D. Whalley, J.M. Skelton, J.M. Frost, A. Walsh, Phonon anharmonicity, lifetimes, and thermal transport in $ch_3nh_3pbi_3$ from many-body perturbation theory, Phys. Rev. B 94 (2016) 220301.

[11] A.N. Beecher, O.E. Semonin, J.M. Skelton, J.M. Frost, M.W. Terban, H. Zhai, A. Alatas, J.S. Owen, A. Walsh, S.J.L. Billinge, Direct observation of dynamic

symmetry breaking above room temperature in methylammonium lead iodide perovskite, ACS Energy Lett. 1 (2016) 880–887.
[12] C.E. Patrick, K.W. Jacobsen, K.S. Thygesen, Anharmonic stabilization and band gap renormalization in the perovskite cssni$_3$, Phys. Rev. B 92 (2015) 201205.
[13] G.E. Jellison Jr., F.A. Modine, Parameterization of the optical functions of amorphous materials in the interband region, Appl. Phys. Lett. 69 (1996) 371–373.
[14] E. Aspnes, D.J.B. Theeten, F. Hottier, Investigation of effective-medium models of microscopic surface roughness by spectroscopic ellipsometry, Phys. Rev. B 20 (1979).
[15] P. Hohenberg, W. Kohn, Inhomogeneous electron gas, Phys. Rev. 136 (1964) B864–B871.
[16] W. Kohn, L.J. Sham, Self-consistent equations including exchange and correlation effects, Phys. Rev. 140 (1965) A1133–A1138.
[17] P. Giannozzi, S. Baroni, N. Bonini, M. Calandra, R. Car, C. Cavazzoni, D. Ceresoli, G.L. Chiarotti, M. Cococcioni, I. Dabo, A.D. Corso, S. de Gironcoli, S. Fabris, G. Fratesi, R. Gebauer, U. Gerstmann, C. Gougoussis, A. Kokalj, M. Lazzeri, L. Martin-Samos, N. Marzari, F. Mauri, R. Mazzarello, S. Paolini, A. Pasquarello, L. Paulatto, C. Sbraccia, S. Scandolo, G. Sclauzero, A.P. Seitsonen, A. Smogunov, P. Umari, R.M. Wentzcovitch, Quantum espresso: a modular and open-source software project for quantum simulations of materials, J. Phys.: Condens. Matter 21 (2009) 395502.
[18] H.J. Monkhorst, J.D. Pack, Special points for brillouin-zone integrations, Phys. Rev. B 13 (1976) 5188–5192.
[19] S. Baroni, S. de Gironcoli, A. Dal Corso, P. Giannozzi, Phonons and related crystal properties from density-functional perturbation theory, Rev. Mod. Phys. 73 (2001) 515–562.
[20] F. Giustino, Materials Modelling Using Density Functional Theory: Properties and Predictions, Oxford University Press, 2014.
[21] E.J. Juarez-Perez, R.S. Sanchez, L. Badia, G. Garcia-Belmonte, Y.S. Kang, I. Mora-Sero, J. Bisquert, Photoinduced giant dielectric constant in lead halide perovskite solar cells, J. Phys. Chem. Lett. 5 (2014) 2390–2394.
[22] A. Poglitsch, D. Weber, Dynamic disorder in methylammonium-trihalogenoplumbates (ii) observed by millimeter–wave spectroscopy, J. Chem. Phys. 87 (1987) 6373–6378.
[23] L. Pedesseau, J.-M. Jancu, A. Rolland, E. Deleporte, C. Katan, J. Even, Electronic properties of 2d and 3d hybrid organic/inorganic perovskites for optoelectronic and photovoltaic applications, Opt. Quantum Electron. 46 (2014) 1225–1232.